Supporting Information

Built-in Single-Ion-Conducting Polymer Bridges for Superior Ion Transport Enabling Long-Life and High-Voltage Lithium-Metal Batteries

*Jiajun Gong [a], Qimin Peng [a], Shunshun Zhao [a], Taolue Wen [a], Haojie Xu [a], Weiting Ma [a], Zhicheng Yao [a], Yong Chen *[b], Guoxiu Wang *[b], and Shimou Chen *[a]*

---

[a] J. Gong, Q. Peng, S. Zhao, T. Wen, H. Xu, W. Ma, Z. Yao, Prof. S. Chen
State Key Laboratory of Chemical Resource Engineering, Beijing Key Laboratory of Electrochemical Process and Technology of Materials, Beijing University of Chemical Technology, Beijing 100029, P.R. China
E-mail: chensm@buct.edu.cn
[b] Y. Chen, Prof. G. Wang
Centre for Clean Energy Technology, University of Technology Sydney, Broadway, Sydney, NSW 2007, Australia
E-mail: yong.chen@student.uts.edu.au; Guoxiu.Wang@uts.edu.au

Experimental

Materials

PVDF:TrFE: CTFE = 64: 27: 9 for electrolytes was purchased from Dongguan Hongfu Plastics Trading Department. $Li_{6.4}La_3Zr_{1.4}Ta_{0.6}O_{12}$ (LLZTO) (300 nm) was purchased from Hefei Kejing Materials Technology Co., Ltd. 2-Acrylamido-2-methylpropane sulfonic acid (AMPS), 2,2'-Azobis(2-methylpropionitrile) (AIBN), and N, N-Dimethylformamide (DMF) were purchased from Adamas. Bis(trifluoromethane) sulfonamide lithium (LiTFSI), lithium difluoro(oxalate)borate (LiDFOB), and lithium nitrate ($LiNO_3$) were purchased from Shanghai Songjing New Energy Technology Co., Ltd. Lithium sulfide (Li_2S) was purchased from Tianjin Xiensi Biochemical Technology Co., Ltd, and sulfur sublimed was purchased from West stock Chemical Co., Ltd. Commercial cathode materials $LiFePO_4$ (LFP), $LiCoO_2$ (LCO), $LiNi_{0.8}Co_{0.1}Mn_{0.1}O_2$ (NCM811), $LiNi_{0.9}Co_{0.05}Mn_{0.05}O_2$ (NCM9055), $Na_3V_2(PO_4)_3$ (NVP), PVDF powder (M_w=1200 000 Da, 5130) and Super P (SP) were purchased from Guangdong Candle New Energy Technology Co., Ltd.

Preparation of A-LLZTO

1 g of LLZTO powder was weighed and placed in a bottle containing an appropriate amount of DMF solvent and dispersed by ultrasonication for one hour, after which 1 g of AMPS powder was added to the bottle, after which vigorous stirring was performed for AMPS to completely remove the residual base (Li_2CO_3) from the surface of the LLZTO particles, In situ generation of the single ionic conductor AMPS-Li on the LLZTO surface, and after 48 h of stirring the precursor liquid was subjected to several centrifugal washes, after which the washed products were Vacuum drying was performed to remove the DMF solvent to obtain the treated LLZTO (named A-LLZTO).

Preparation of PTCLA

In a vial, 0.4 g of PTC, 0.08 g of A-LLZTO, 0.2 g of LiTFSI, and 0.001 g of AIBN were accurately weighed, respectively. Subsequently, 2.5 g to 2.6 g of DMF was added to the vial. The mixture was then heated at 60 °C and stirred for 24 h, ensuring the polymerization of AMPS-Li to PAMPS-Li on the LLZTO surface, followed by continuous stirring at room temperature for an additional 24 h. The precursor liquid was then degassed under vacuum to remove air bubbles, after which it was carefully coated onto a glass plate. The coated plate was placed in a vacuum-drying oven at 50 °C for 24 h. The resulting dried electrolyte film, designated as PTCLA, was cut into small discs with a diameter of 16 mm and stored in a glove box for future use. Additionally, all electrolytes were stored in the glove box for at least 4 days before their utilization.

Preparation of PTCL and PTC SPE

Preparation of PTCL: PTC/DMF solution with a mass fraction of 12.5%. Weigh 0.08 g of LLZTO without any treatment and 0.2 g of LiTFSI into a vial, add 2 g of DMF, and ultrasonic for half an hour for dispersion. Then 3.2 g of PTC/DMF solution was added, stirred for 7 h, and then scraped on a glass plate, dried to form a film, and then cut into 16mm diameter discs and put into a glove box for spare.

Preparation of PTC SPE: Weigh 0.4 g of PTC powder and 0.2 g of LiTFSI, and add 2.5−2.6 g of DMF solution for stirring, stirring until clarified and transparent scraping coated on a smooth glass plate. After drying to form a film, cut into round pieces with a diameter of 16 mm and put into the glove box for spare.

Preparation of PTCNA

First, 1 g of NASICON filler was ultrasonically dispersed in DMF, followed by the addition of 1 g of AMPS under vigorous stirring. After stirring for 24 h, the filler was collected by centrifugation, washed thoroughly, and vacuum-dried to obtain the modified NASICON filler. Subsequently, 0.4 g of PTC powder, 0.22 g of sodium bis(trifluoromethanesulfonyl)imide (NaTFSI), and 0.08 g of the modified NASICON filler were weighed and placed into a vial. An appropriate amount of DMF was added, and the mixture was stirred at 50 °C for 2 h, followed by further stirring at room temperature for 12 h. After removing bubbles from the resulting precursor solution under vacuum, the solution was cast onto a smooth glass plate and subjected to drying in a vacuum oven at 50 °C. Finally, the dried film was cut into small discs with a diameter of 16 mm and stored in an argon-filled glove box for further use.

Preparation of cathodes and treatment of electrode/electrolyte interface.

All the cathodes were prepared according to the ratio of the active substance: PVDF: SP=8:1:1, the positive electrode was added with the appropriate amount of NMP and stirred overnight, scraped, and coated on aluminum foil, heated at 80 °C for 12 h and then cut into 10 mm small discs and put into the glove box for spare parts, all the cathode loadings were in the range of 1.9−2.6 mg cm^{-2}, except for NVP cathode (1.274 mg cm^{-2}). To mitigate the issue of poor contact between the electrolyte and the electrode, a minimal amount of liquid electrolyte (LE) (5 μL) is applied to wet the electrode/electrolyte interface. The LE preparation method for interfacial wetting:

Firstly, we synthesized lithium thiocarbonate (LTC) as an additive, based on the reported work.[S1] To synthesize LTC, 0.015 g of Li_2S and 0.15 g of sublimated sulfur were accurately weighed and placed in a vial. Subsequently, 0.43 g of LiDFOB (1 mol L^{-1}) and 0.207 g of $LiNO_3$ (0.1 mol L^{-1}) were added as lithium salts. Following this, 0.5 mL of FEC, 0.5 mL of PC, 1 mL of DEC, and 1 mL of EMC were added sequentially. The mixture was then vigorously stirred at room temperature for 48 h. Upon completion of the reaction, the solution was allowed to stratify naturally, and the supernatant was carefully collected to serve as the electrolyte for wetting the electrode/electrolyte interface.

In the experiment of the pouch cell lighting up the light board, the size of the cathode was 3 cm×4 cm and the positive active material loading was 10.5 mg cm^{-2}. The light board by the pouch cell experiment has an operating voltage of 1.5 V, a pixel array of 11×44 dots, and dimensions of 93 mm×30 mm×6 mm.

Characterizations

The crystalline phase analysis of powders and membranous was performed using X-ray diffraction (XRD, Bruker D8 Focus), ranging from 10−90° with a scan rate of 5°

min^{-1}. The Fourier Transform Infrared (FT-IR) spectroscopy measurement of the materials was conducted on a Nicolet 6700 (Thermo Fisher, USA). X-ray photoelectron spectroscopy (XPS) was obtained by Thermo Scientific K-Alpha instrument. Electron Paramagnetic Resonance (EPR) testing of ceramic powders was conducted on a Bruker-EmxPlus in Germany. Raman spectroscopy was recorded at room temperature using InVia Reflex with laser excitation at 785 nm. Solid-state magic angle spinning ^{7}Li NMR was performed using a Bruker 400WB AVANCE III instrument. The surface morphology of the oxide nanofillers and the morphology at the cathode side were analyzed by transmission electron microscopy (TEM, JEOL HEM-ARM200F). The morphology and structure of the electrolyte film and anode were characterized using field emission scanning electron microscopy (SEM, Zeiss Supra 55VP) with an accelerating voltage of 5 kV. Thermogravimetric analysis (TGA) was performed using a TGA5500 under a nitrogen atmosphere with a temperature range of 40 ~ 800 °C and a ramp rate of 10 °C min^{-1}. X-ray absorption fine structure spectra (XAS) were collected at the Australia National Synchrotron Radiation Research Centre and analyzed using the ATHENA software package.[S2]

Density functional theory (DFT) calculations

The DFT calculations were performed using the Gaussian16 program package[S3] with the b3lypp-d3 def2-TZVP basis set.[S4] Quantum chemical calculations of HOMO and LUMO energies were carried out using density functional theory.

Calculation of Li$^+$ migration in the surface layer of LLZTO: The simulations were carried out utilizing the density functional theory (DFT) framework as incorporated in the Quantum Espresso package (QE).[S5, 6] The generalized gradient approximation (GGA) with the Perdew-Burke-Ernzerhof (PBE) functional was utilized to describe the exchange-correlation energies.[S7, 8] The pseudo-potentials for the specific atoms were generated using the projected augmented wave (PAW) method, [S9] and the criteria for convergence were established at 0.02 eV/Å for the maximum force and 10^{-5} eV for the energy per atom during the structure relaxation process. The sampling of the Brillouin zone was performed using Monkhorst-Pack (MP) grids, with special points separated by 0.04 Å-5 eV for the total energy and 0.02 eV/Å for the ionic forces. To account for the physical van der Waals (vdW) interactions in our calculations, a semi-empirical DFT-D3 force-field approach was employed.

The adsorption energy (Eb) was calculated based on the following Eq. (1):

$$E_b = E_{t1} - E_{s1} - E_{s2} \tag{1}$$

Where E_{t1} is the total energy of the binding system, E_{s1} is the energy of the optimized clean bulks, and E_{s2} is the energy of the adsorbates in a vacuum.[S8-10]

For the identification of transition states, we employed the climbing image nudged elastic band (CI-NEB) method, which is integrated into the transition state tools of the Quantum Espresso (QE) package.[S10] The interpolated images underwent full relaxation until a force convergence criterion of 0.05 eV/Å was met. The CI-NEB method represents an enhancement over the conventional NEB approach, exhibiting greater efficiency in determining the minimum energy path through linear interpolation of the reaction coordinates.

Electrochemical measurements

The model of the cell is C2025. The Autolab electrochemical workstation (manufactured by Metrohm, Switzerland) was utilized to measure ionic conductivity, linear sweep voltammetry (LSV), cyclic voltammetry (CV), and electrochemical impedance spectroscopy (EIS). LSV is measured by assembling a Li||SS cell, the voltage range tested was 2.5–7.5 V (V vs Li/Li^+), with a scanning speed of 0.05 mV s^{-1}. The EIS was performed with 10 mV of AC amplitude over the frequency range from 0.1 Hz to 100000 Hz. The ionic conductivity was conducted at room temperature in a coin cell with symmetrical stainless steel (SS) electrodes. The following Eq.(2) was used to calculate the ionic conductivity of electrolytes.

$$\sigma = L/R \cdot S \tag{2}$$

Where σ is the ionic conductivity, L is the distance between two pieces of stainless steel, S is the contact area between the electrolyte and stainless steel, and R is the bulk resistance. The electrical conductivity of the solid electrolyte is calculated using the Eq. (3):

$$\sigma_e = I_s L / US \tag{3}$$

Where U is the potential; I_S is the steady state current; L is the thickness; and S is the surface area of SPE.

The lithium-ion transference numbers (LTN) of electrolytes were tested on a 2025-type coin sandwiching the electrolytes between two Li by AC impedance and DC polarization. Where the polarization currents (initial (I_0) and steady state (I_{ss})) were measured under a DC polarization voltage of 50 mV (ΔV). The impedances before and after polarization are R_0 and R_{ss}, respectively. Then, the LTN was calculated according to the Bruce–Vincent–Evans equation as Eq.(4).

$$LTN = I_{ss}(\Delta V - I_0 R_0)/I_0(\Delta V - I_{ss} R_{ss}) \tag{4}$$

The long cycling performance of Li||Li symmetric cells, Li||LFP (1 C=170 mAh g^{-1}), Li||LCO (1 C=175 mAh g^{-1}), Li||NCM811 (1 C=180 mAh g^{-1}), Li||NCM9055 (1 C=188 mAh g^{-1}), Na||NVP (1 C=117 mAh g^{-1}), and Na||NVPF (1 C=128 mAh g^{-1}) cells were performed on the Neware Battery Measurement System, and LAND CT2001A battery test system. All the coin cells and pouch cells underwent a three-cycle (0.1 C) activation step before the long-cycle test. In particular, for cycle testing at low temperatures, two cycles of activation at a rate of 0.1 C were performed at room temperature before transferring to low temperatures to continue activation for one cycle (0.1 C).

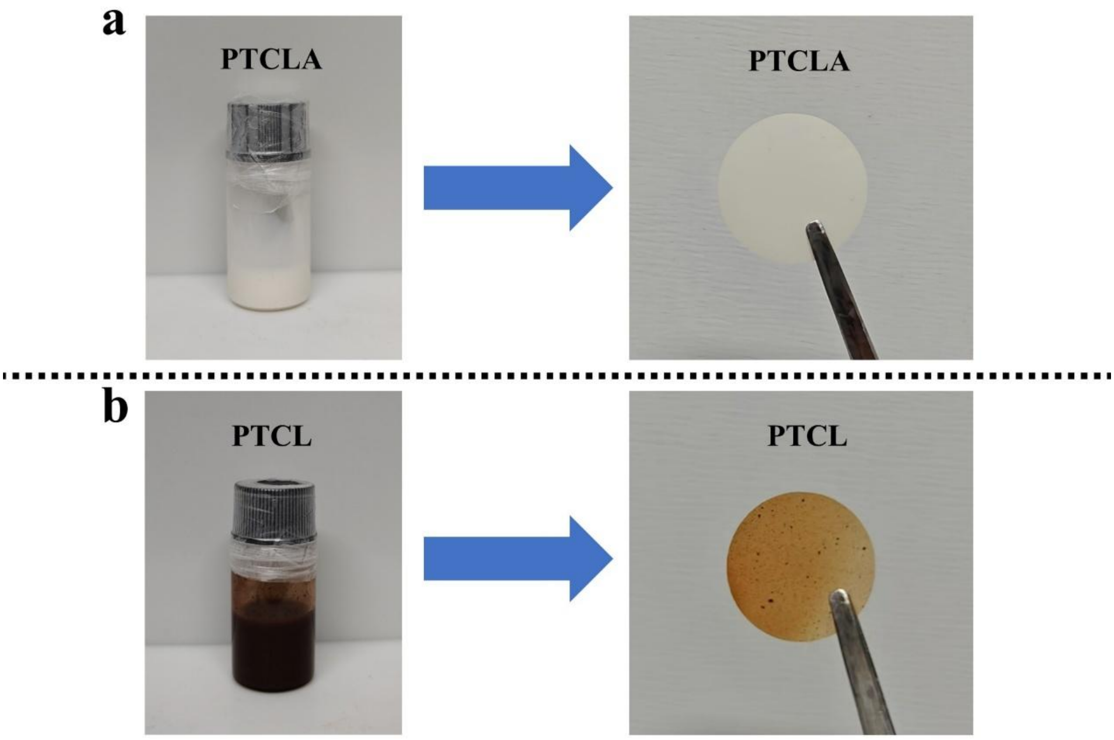

Fig. S1 The slurry and membrane images of (a) PTCLA and (b) PTCL.

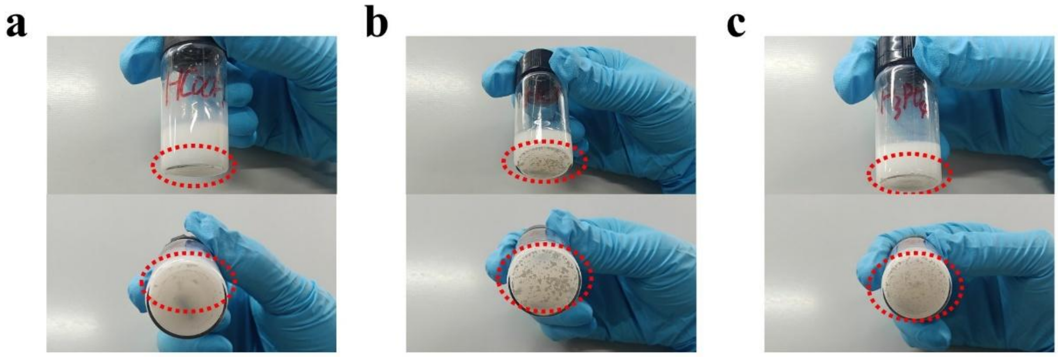

Fig. S2 Images of the slurry prepared by compounding pristine LLZTO treated with (a) formic acid, (b) hydrochloric acid, and (c) phosphoric acid, with PTC.

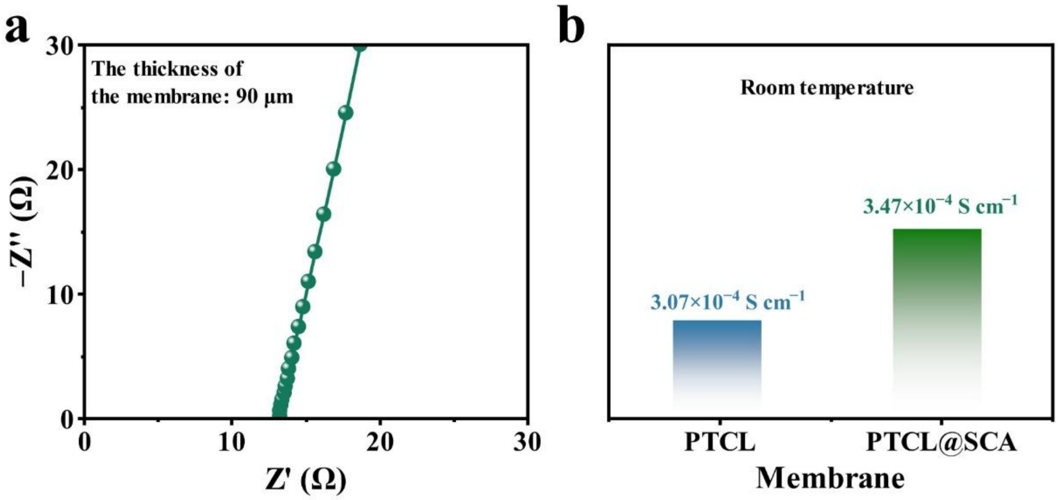

Fig. S3 The steps for modifying LLZTO with a silane coupling agent were followed by reported work,[S11] and the modified LLZTO was then composited with PTC (designated as PTCL@SCA). (a) The EIS curve of PTCL@SCA, and (b) The bar chart comparing the ionic conductivity of PTCL and PTCL@SCA.

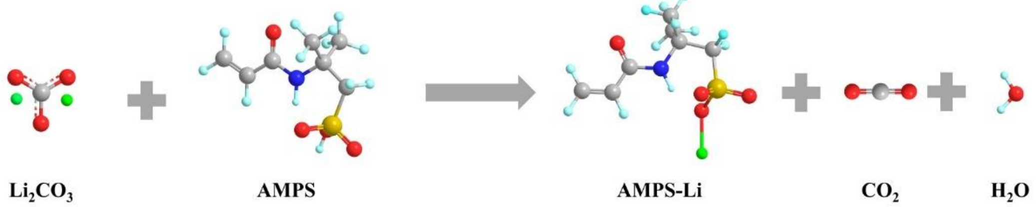

Fig. S4 Reaction equation for the in-situ generation of single ionic conductors at the surface during AMPS treatment of LLZTO.

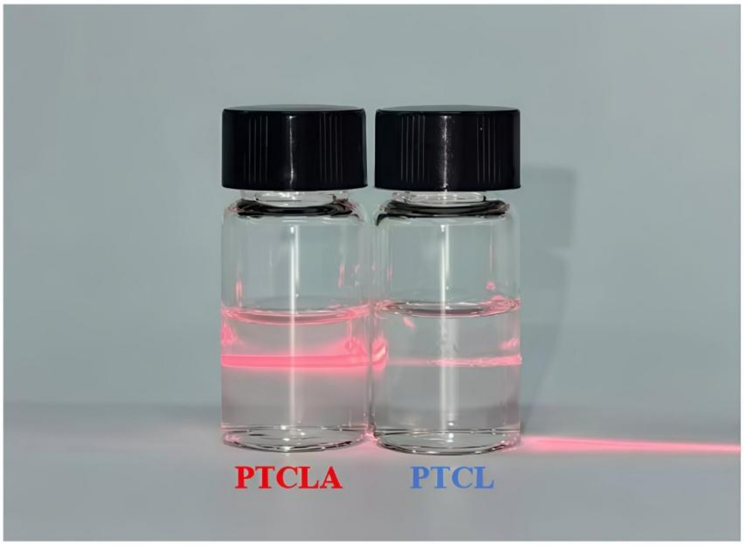

Fig. S5 Tyndall effect observed by dispersing pristine LLZTO and A-LLZTO in isopropanol solution, respectively.

Note: The pristine LLZTO and A-LLZTO powders were dispersed separately in isopropanol solutions to observe the dispersion of the fillers therein, as shown in Fig. S5. When light was passed through the two solutions, it was observed that the light transmitted through the solution containing A-LLZTO was finer compared to that through the pristine LLZTO solution, indicating that A-LLZTO exhibited better dispersion capability than pristine LLZTO.

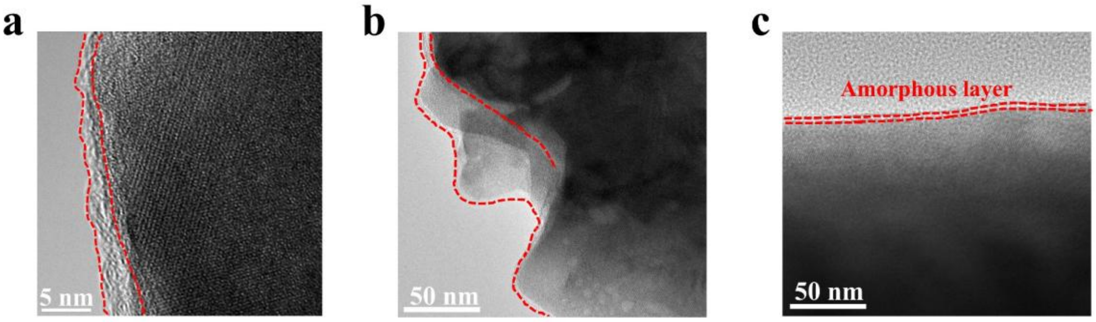

Fig. S6 (a) and (b) are TEM images of pristine LLZTO; (c) is a TEM image of A-LLZTO.

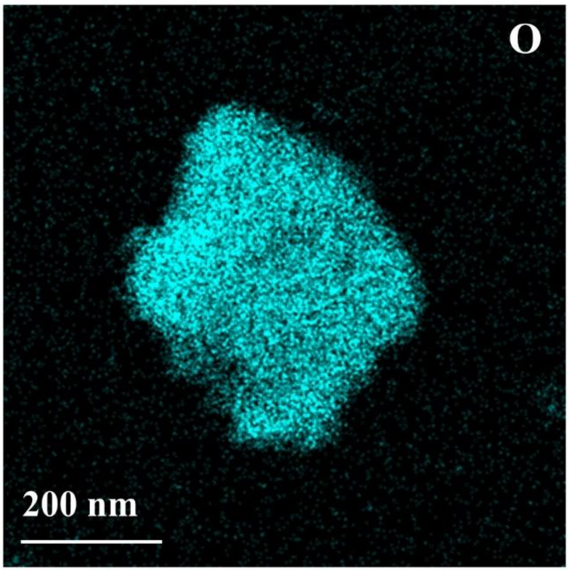

Fig. S7 The TEM mapping of oxygen element in A-LLZTO.

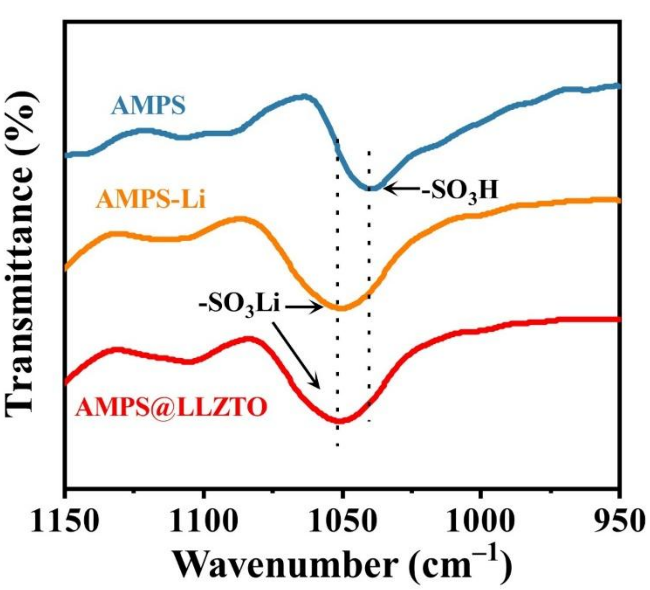

Fig. S8 FT-IR spectra of the pristine LLZTO and A-LLZTO samples, respectively.

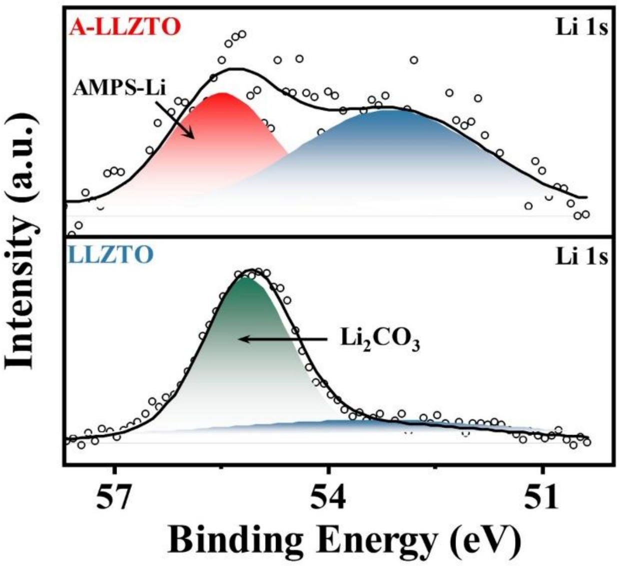

Fig. S9 XPS spectra of the pristine LLZTO and A-LLZTO samples of Li 1s.

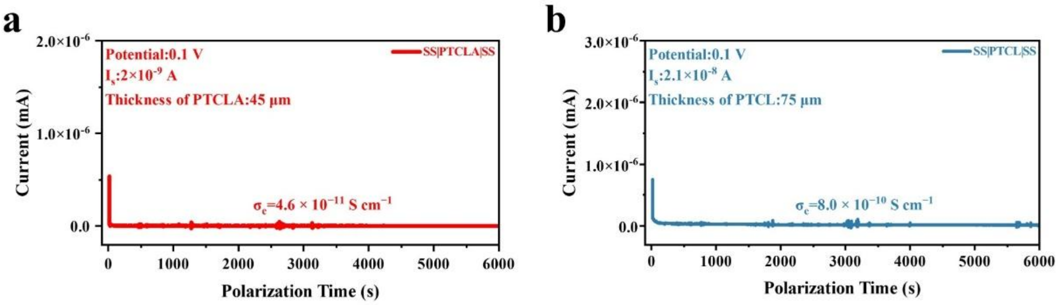

Fig. S10 Electronic conductivity testing of (a) PTCLA and (b) PTCL electronic conductivity testing of (a) PTCLA and (b) PTCL.

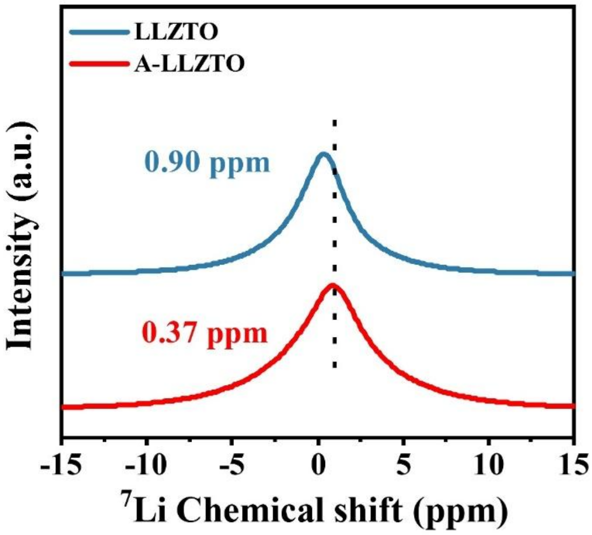

Fig. S11 ^{7}Li solid-state Nuclear Magnetic Resonance spectra of pristine LLZTO and A-LLZTO.

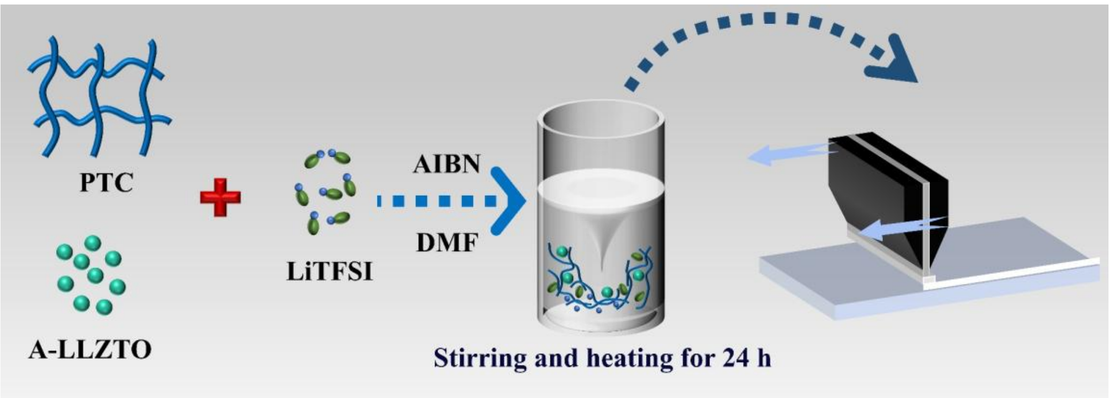

Fig. S12 Schematic flow diagram illustrating the preparation process of the PTCLA electrolyte.

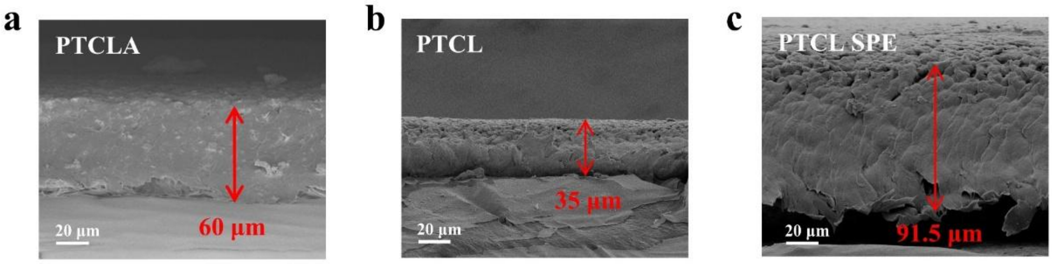

Fig. S13. Cross-sectional SEM images of (a) PTCLA, (b) PTCL, and (c) PTC SPE membranes.

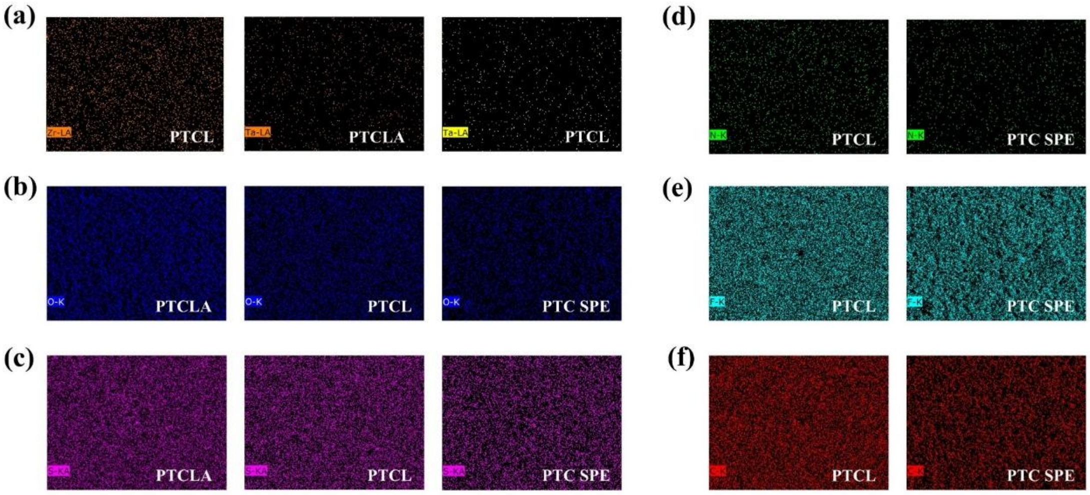

Fig. S14 (a) EDS maps of Zr and Ta in PTCL and the Ta in PTCLA. (b) O and (c) S are EDS images of three samples: PTCLA, PTCL, and PTC SPE, respectively. (d) N, (e) F, and (f) C elements are EDS images of two samples: PTCL and PTC SPE, respectively.

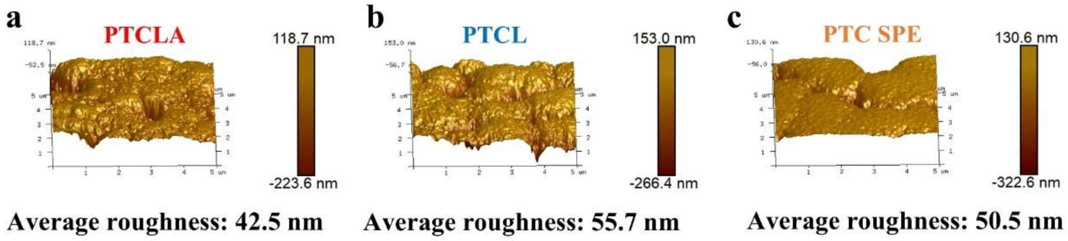

Fig. S15 Surface roughness of various electrolytes measured by AFM. (a) PTCLA, (b) PTCL, (c) PTC SPE.

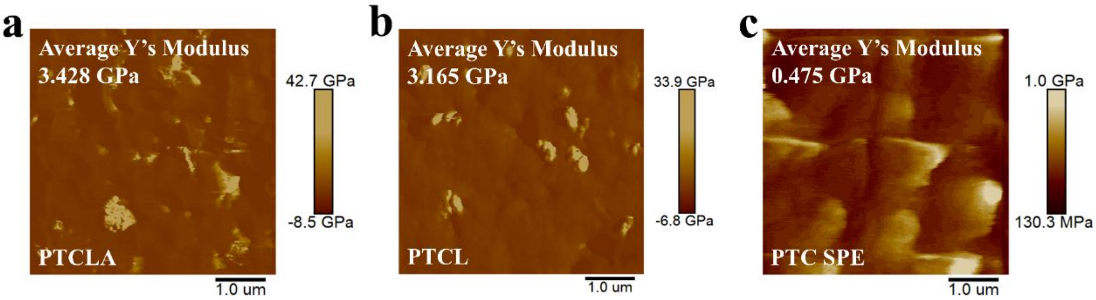

Fig. S16 AFM and corresponding Young's modulus test of various electrolytes. (a) PTCLA, (b) PTCL, and (c) PTC SPE.

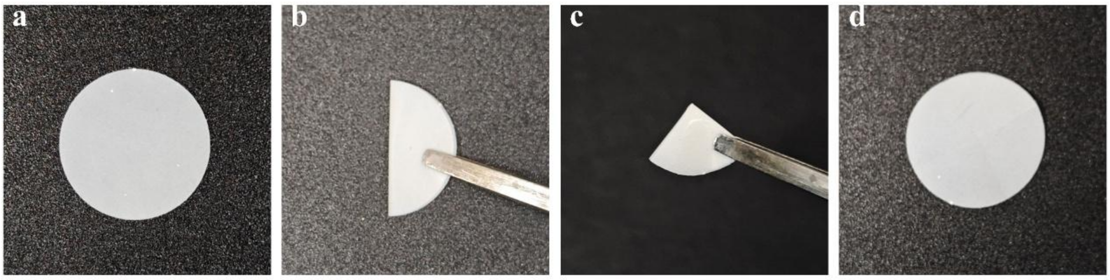

Fig. S17 Photographs of PTCLA with different folded shapes. (a) flatten, (b) fold, (c) bifold, (d) flatten.

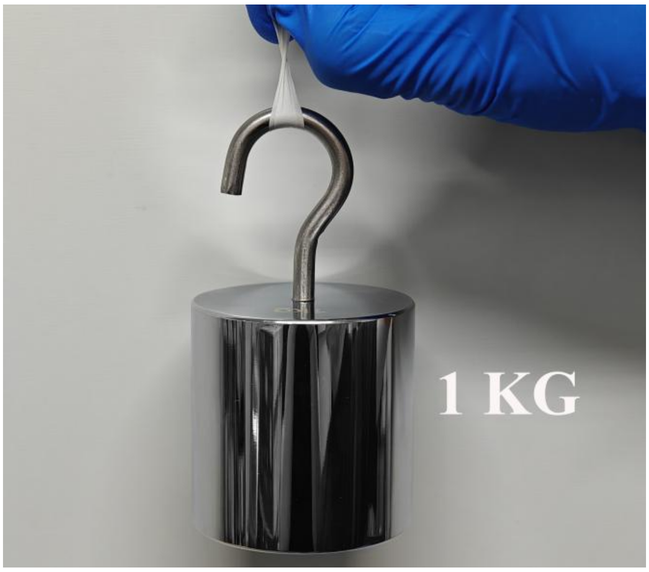

Fig. S18 Photograph of PTCLA, supporting hanging 1 kg weights.

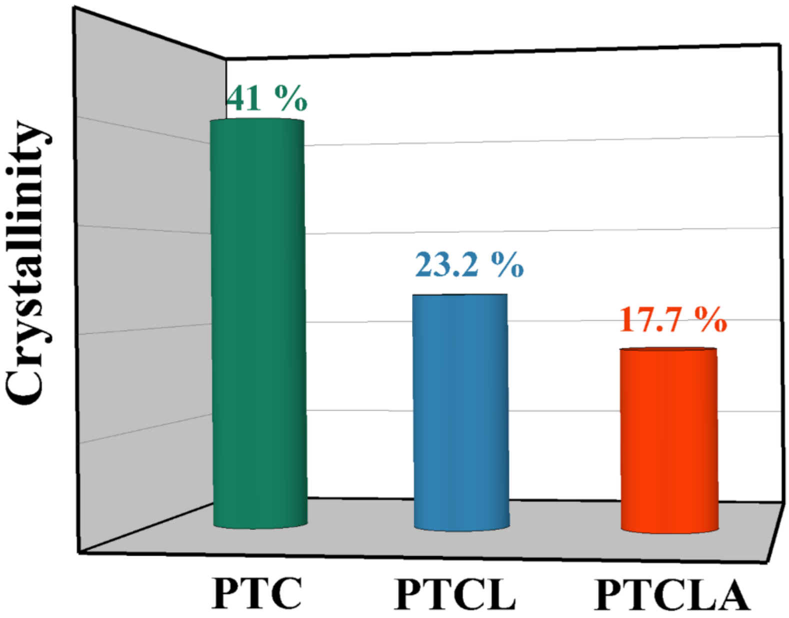

Fig. S19 The crystallinity of PTCLA, PTCL, and PTC.

Note: The calculation steps: First, based on the obtained XRD curve, calculate the total area under the curve through integration. Then, determine the area of the crystalline peaks of the polymer by integrating them individually. Finally, divide the area of the crystalline peaks by the total area to obtain the ratio of the crystalline region in the XRD curve.

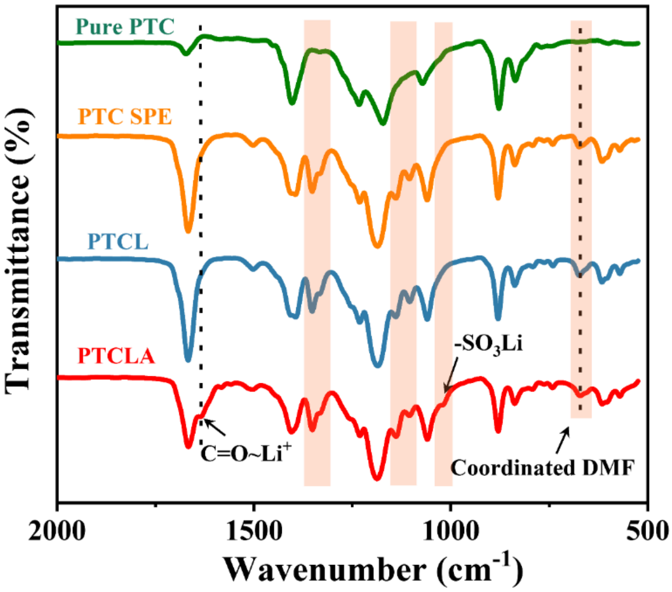

Fig. S20 FT-IR of PTCLA, PTCL, PTC SPE, and pure PTC.

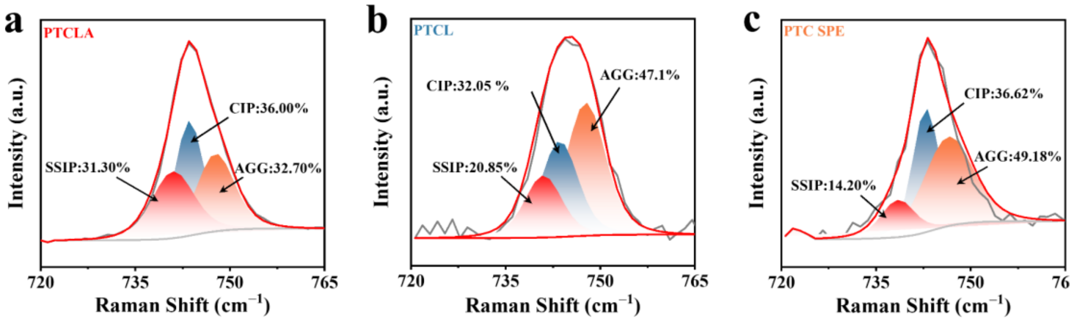

Fig. S21 Raman spectra of (a) PTCLA, (b) PTCL, and (c) PTC SPE at 725–765 cm^{-1} (in which SSIP is solvent-separated ion pairs, CIP is contact ion pairs, and AGG is aggregated).

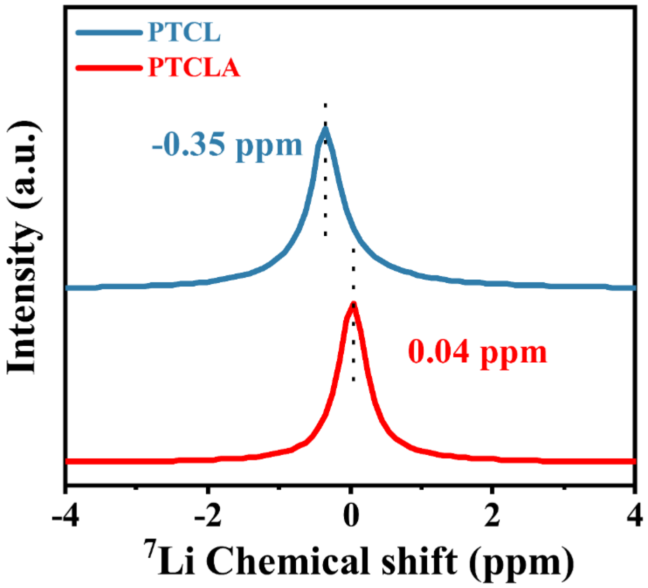

Fig. 22 ^{7}Li solid-state NMR spectra of PTCLA and PTCL.

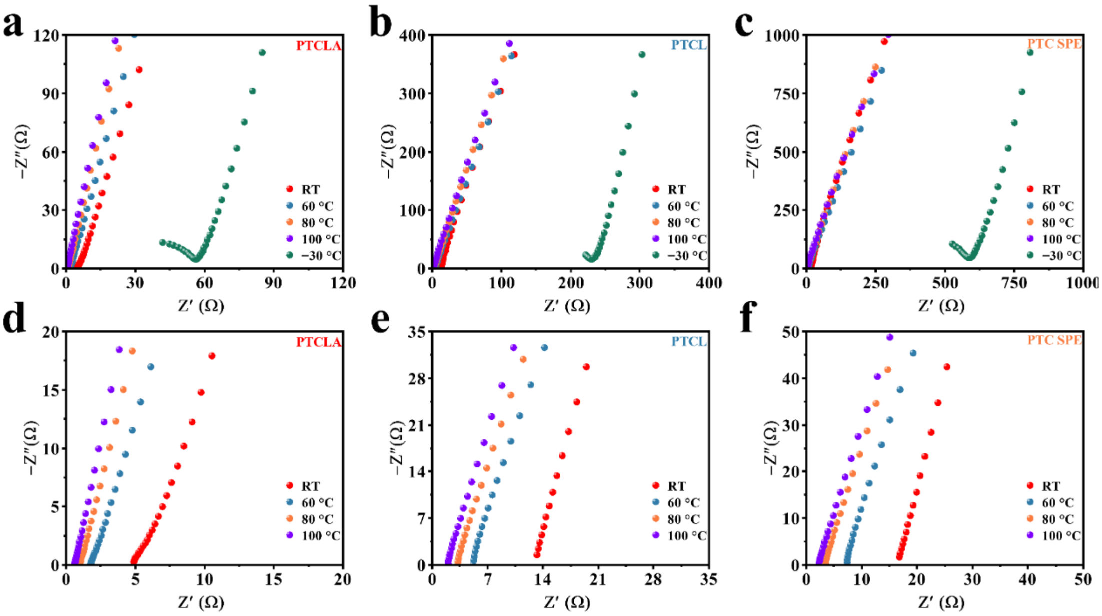

Fig. S23 The EIS curve of (a, d) PTCLA, (b, e) PTCL, (c, f) PTC SPE from −30 °C to 100 °C. Herein, (d), (e), and (f) are the locally enlarged views of the EIS curves for PTCLA, PTCL, and PTC SPE, respectively.

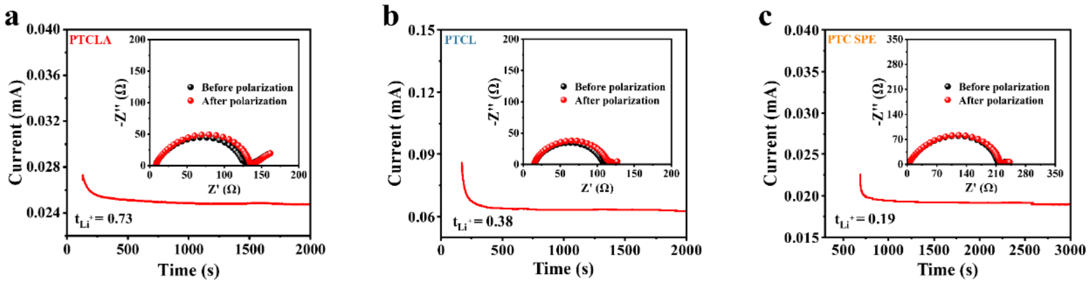

Fig. S24 The LTN of (a) PTCLA, (b) PTCL, and (c) PTC SPE.

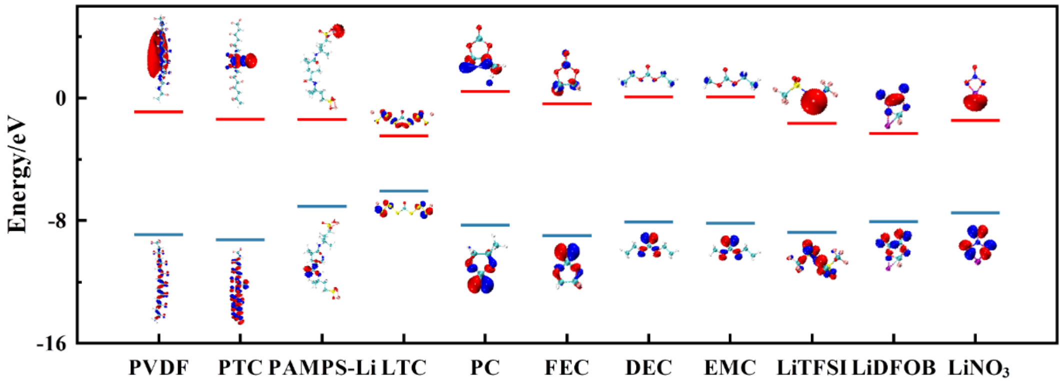

Fig. S25 Theoretical calculations of LUMO/HOMO for PVDF, PTC, PAMPS-Li, LTC, PC, FEC, DEC, EMC, LiTFSI, LiDFOB, and $LiNO_3$.

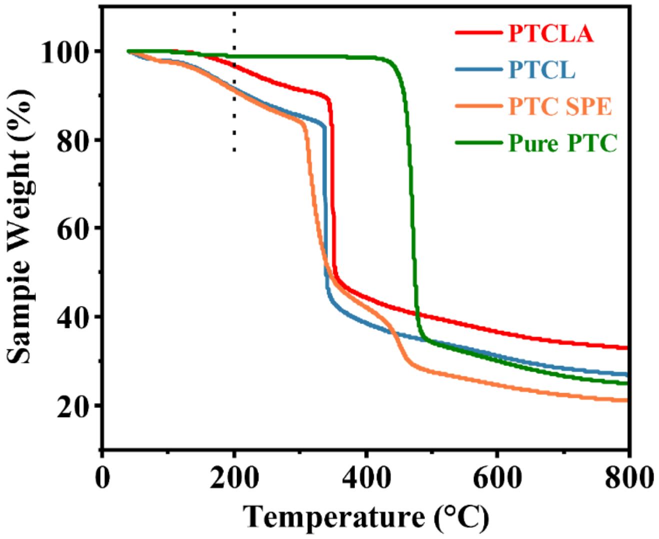

Fig. S26 TGA curves of PTCLA, PTCL, PTC SPE, and pure PTC.

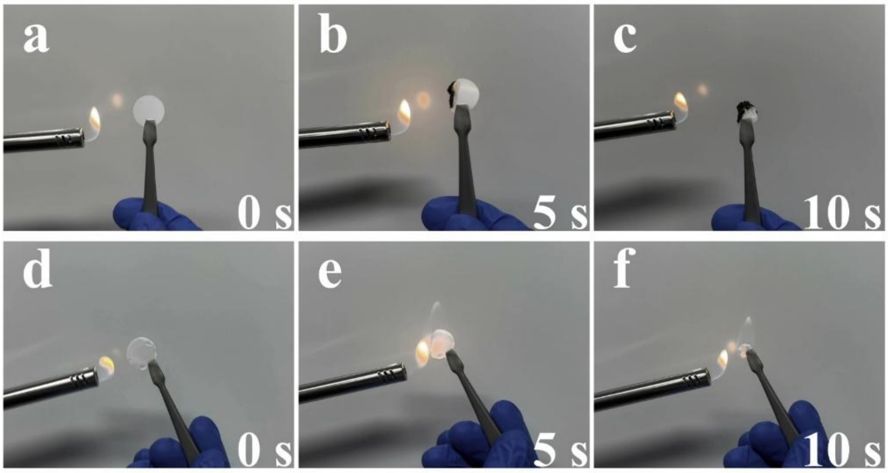

Fig. S27 Combustion test. (a-c) PTCLA, (d-f) Celgard separator immersed with LEs.

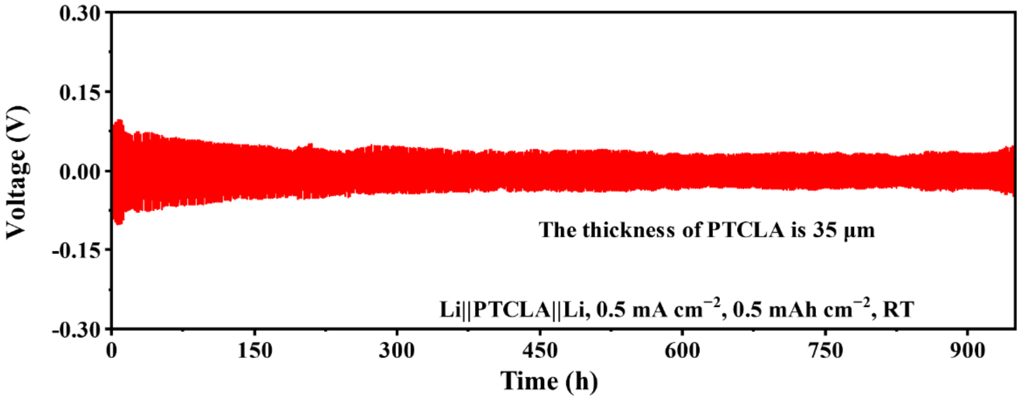

Fig. S28 Cycling performances of Li||Li symmetric cell with PTCLA (35 μm) at 0.5 mA cm^{-2}.

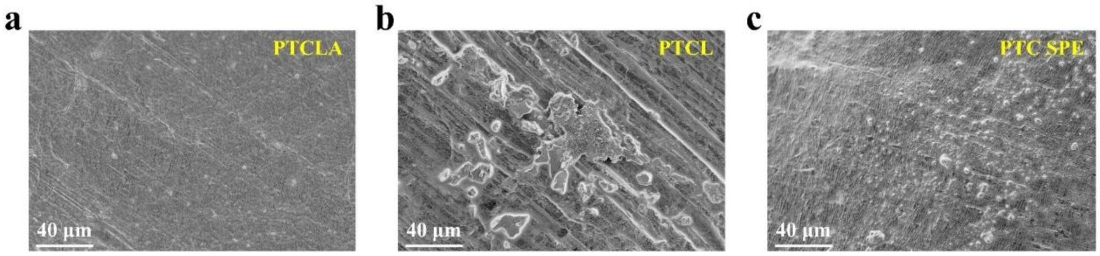

Fig. S29 SEM image of (a) Li|PTCLA|Li, (b) Li|PTCL|Li, and (c) Li|PTC SPE|Li cells after 50 cycles at 0.5 mA cm^{-2}.

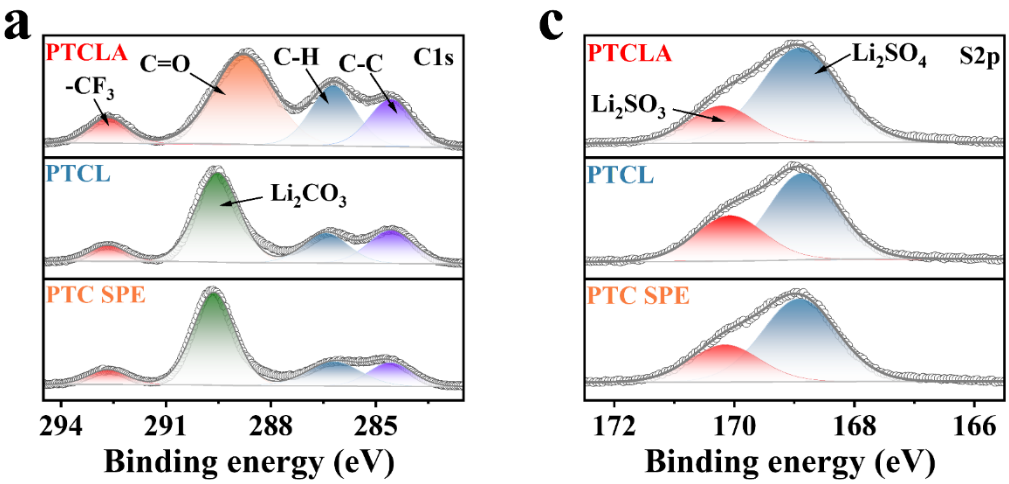

Fig. S30 XPS compositional analysis of Cu electrode surfaces after cycling of Li||Cu cells assembled using PTCLA, PTCL, and PTC SPE. (a) C 1s, (b) S 2p.

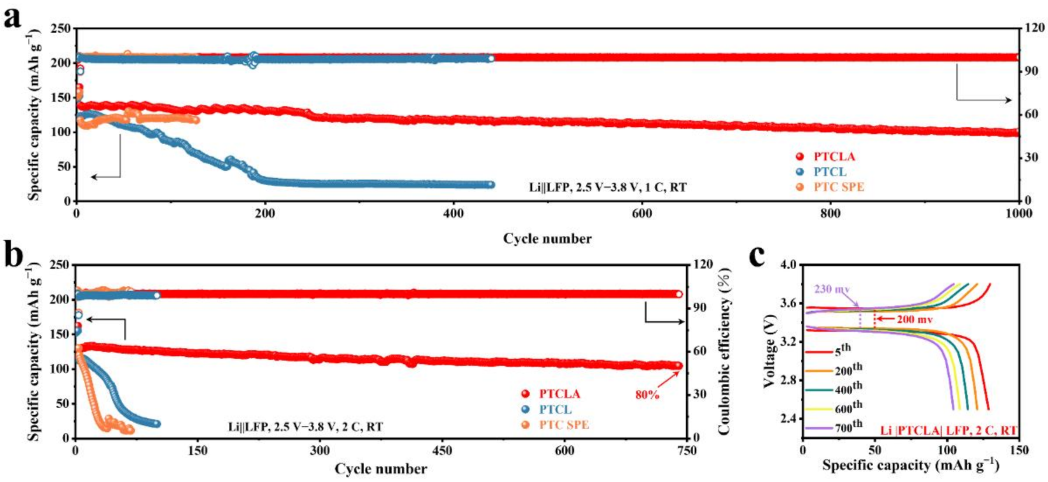

Fig. S31 Cycle performances of Li|PTCLA|LFP cells at (a) 1 C and (b) 2 C; (c) Charge-discharge voltage profiles of Li|PTCLA |LFP cells at 2 C.

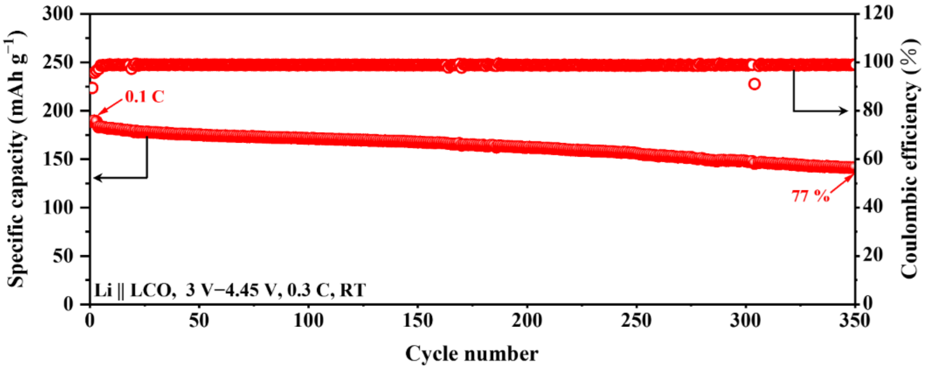

Fig. S32 Cycle performances of Li|PTCLA|LCO cells at 0.3 C (4.45 V) and RT.

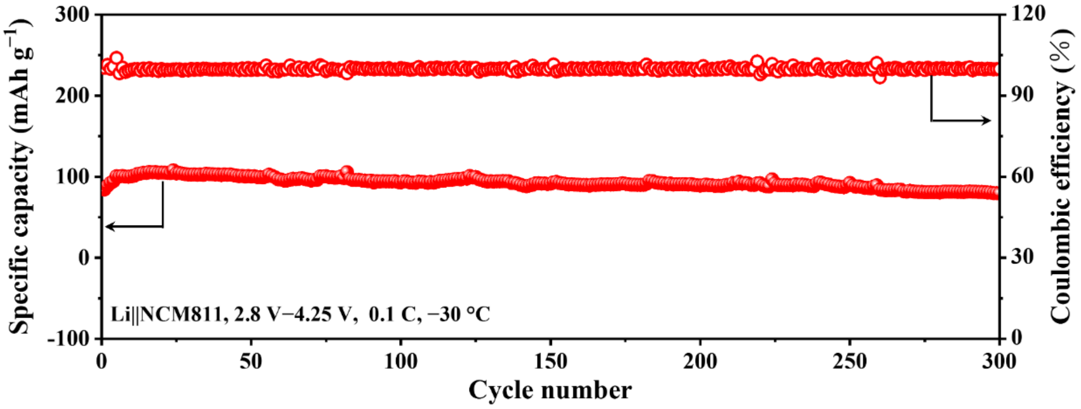

Fig. S33 Cycle performances of Li|PTCLA|NCM811 cells at −30 °C.

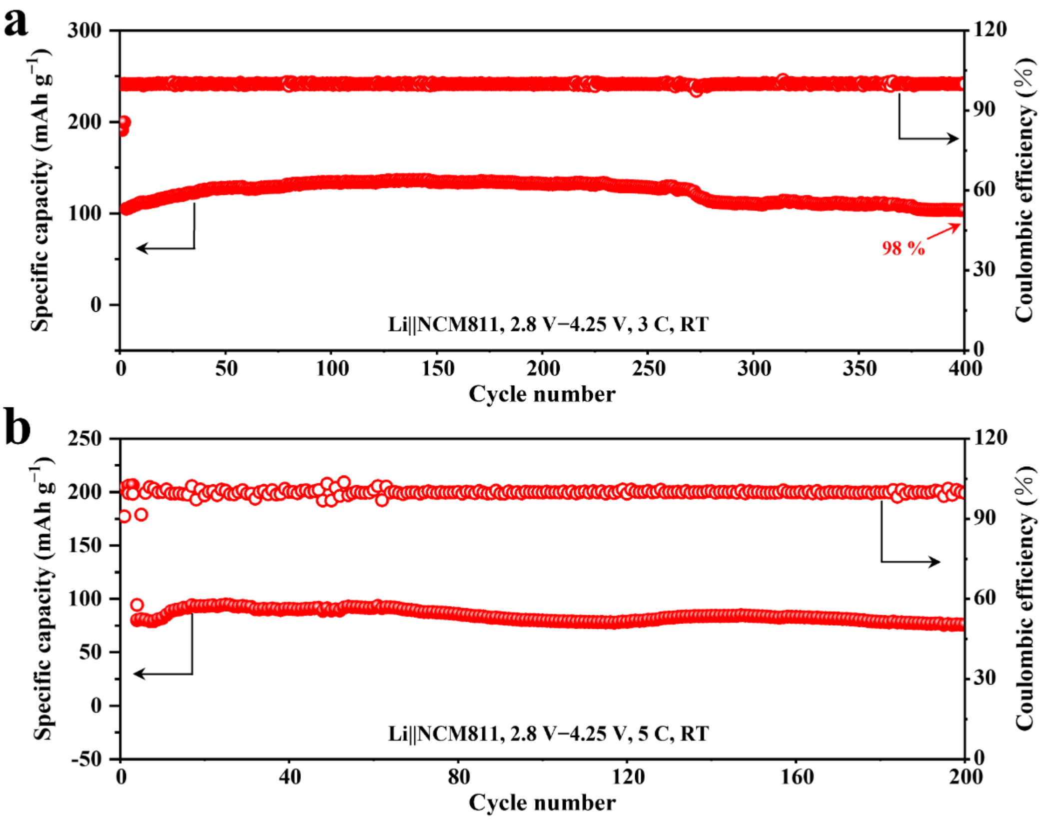

Fig. S34 Cycle performances of Li|PTCLA|NCM811 cells at (a) 3 C and (b) 5 C.

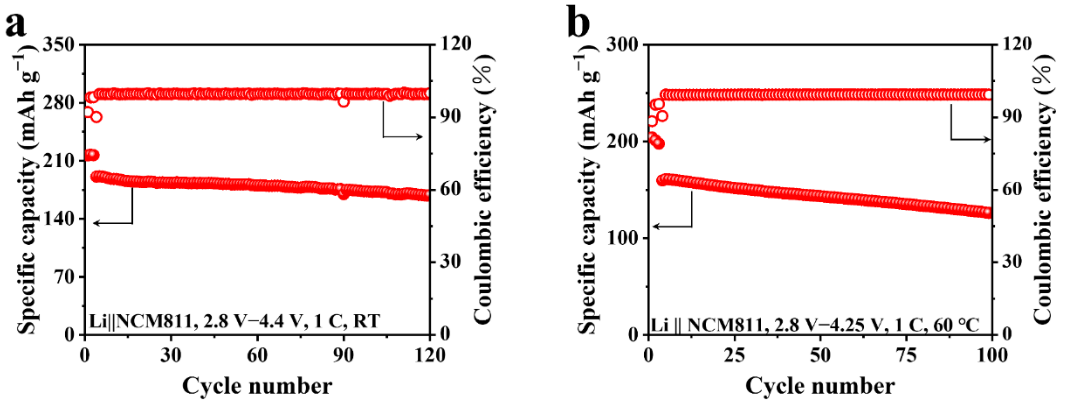

Fig. S35 Cycle performances of Li|PTCLA|NCM811 cells at (a) 4.4 V (RT) and (b) 4.25 V (60 °C).

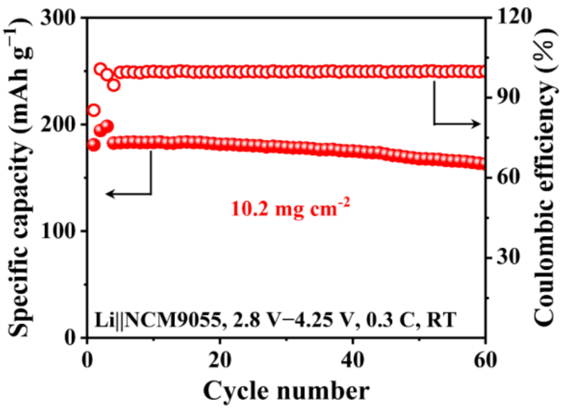

Fig. S36 Cycle performances of Li|PTCLA|NCM9055 cells at the cathode with high active material loading (10.2 mg cm^{-2}).

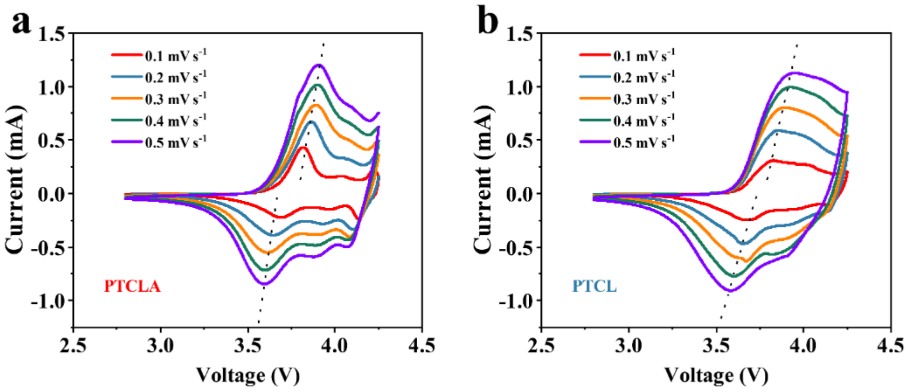

Fig. S37 CV curves of (a) Li|PTCLA|NCM9055 and (b) Li|PTCL|NCM9055 cells. The scan rate is 0.1–0.5 mV s^{-1}.

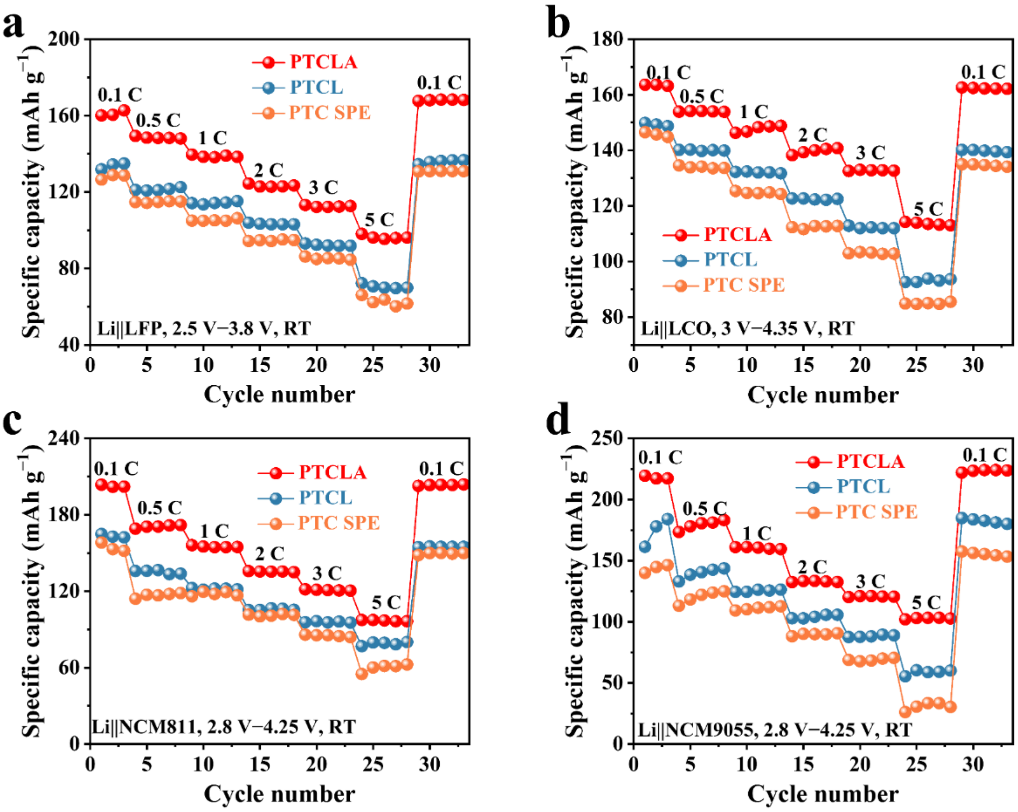

Fig. S38 Cycling performance of (a) Li||LFP cells, (b) Li||LCO cells, (c) Li||NCM811 cells, and (d) Li||NCM9055 cells at 0.1 to 5 C at RT.

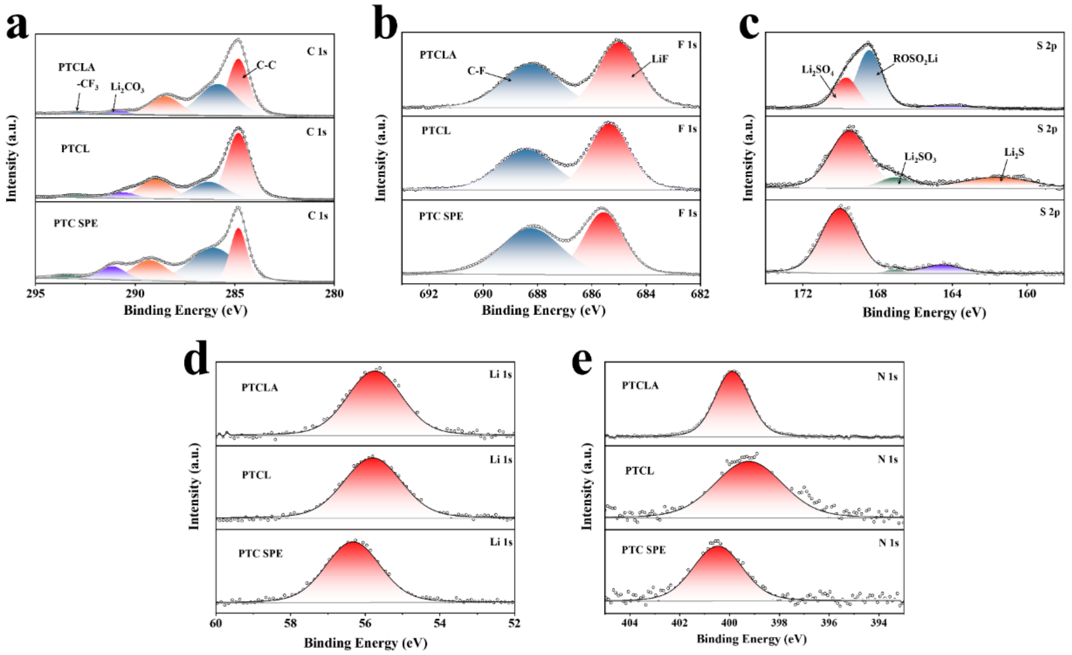

Fig. S39 XPS compositional analysis of cathode surfaces after cycling of Li||NCM9055 cells assembled using PTCLA, PTCL, and PTC SPE. (a) C 1s, (b) F 1s, (c) S 2p, (d) Li 1s, and (e) N 1s.

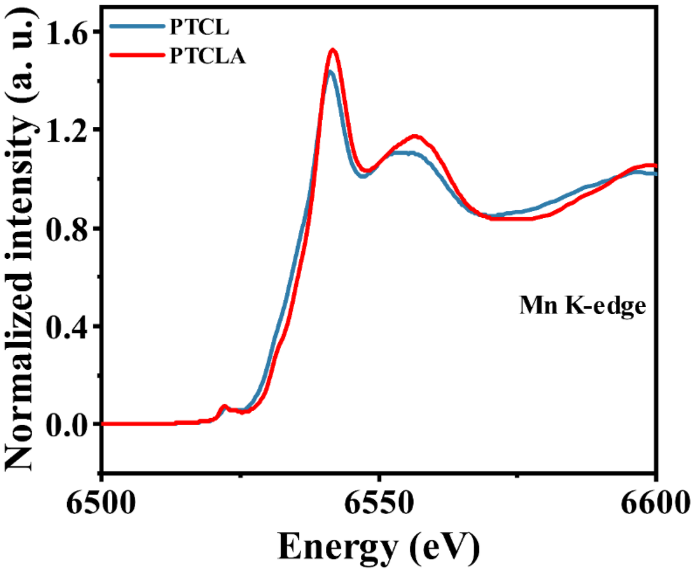

Fig. 40 Mn K-edge XANES spectra of NCM9055 cathodes after cycling of Li|PTCLA|NCM9055 and Li|PTCL|NCM9055 cells.

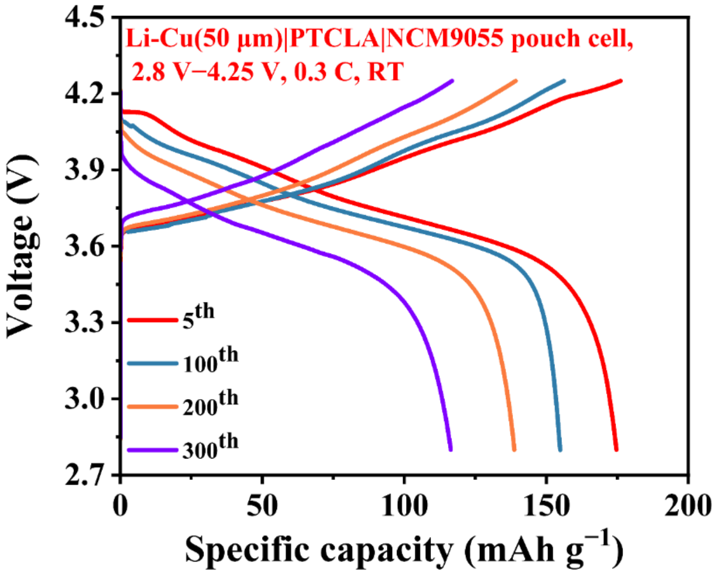

Fig. S41 The charge-discharge voltage profiles of Li-Cu(50 μm)|PTCLA|NCM9055 pouch cells at 0.3 C.

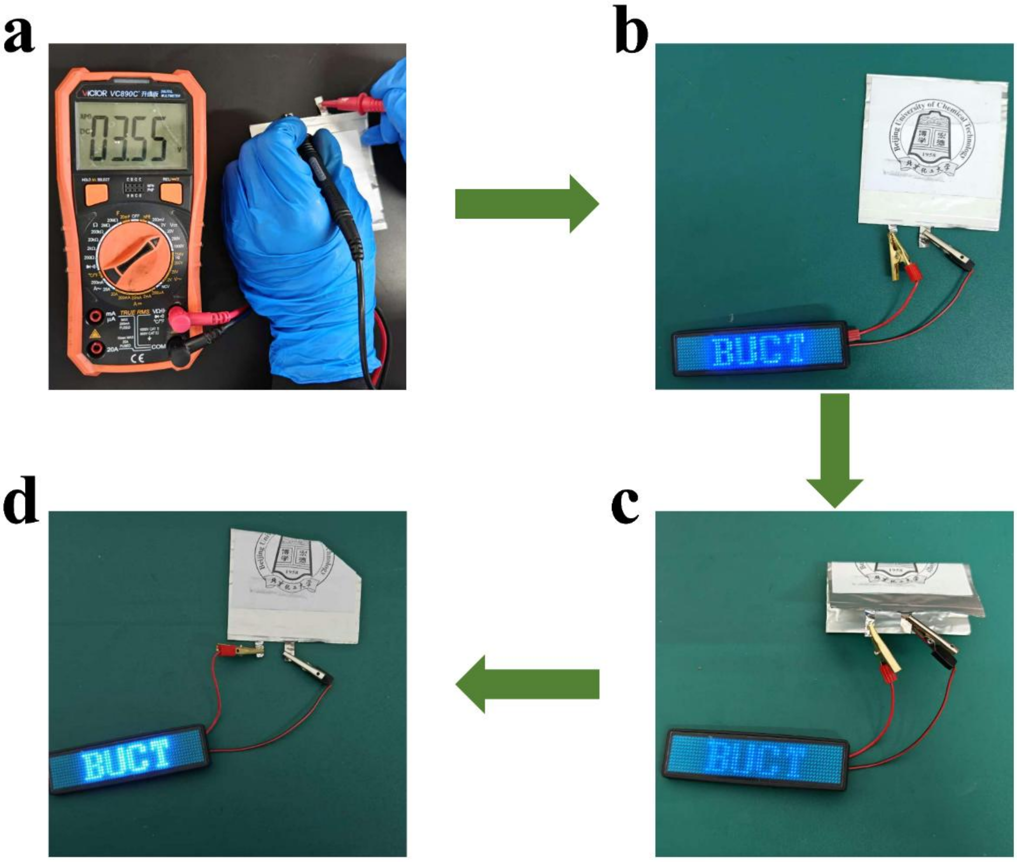

Fig. S42 (a) Open circuit voltage of the pouch cell. Pictures of Li|PTCLA|NCM9055 pouch cells in (b) normal state, (c) folded, and (d) cut to light the light panel.

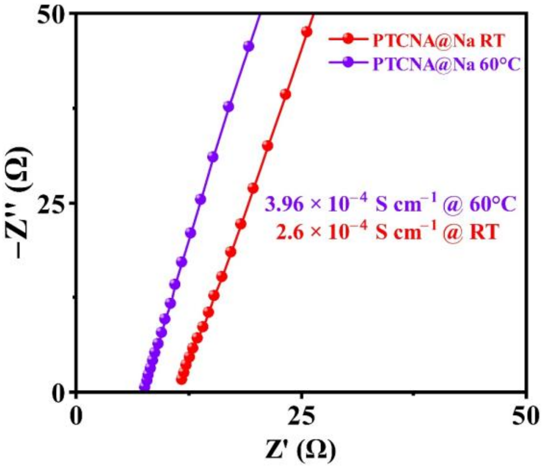

Fig. S43 The EIS curve of PTCNA@Na at RT and 60 °C.

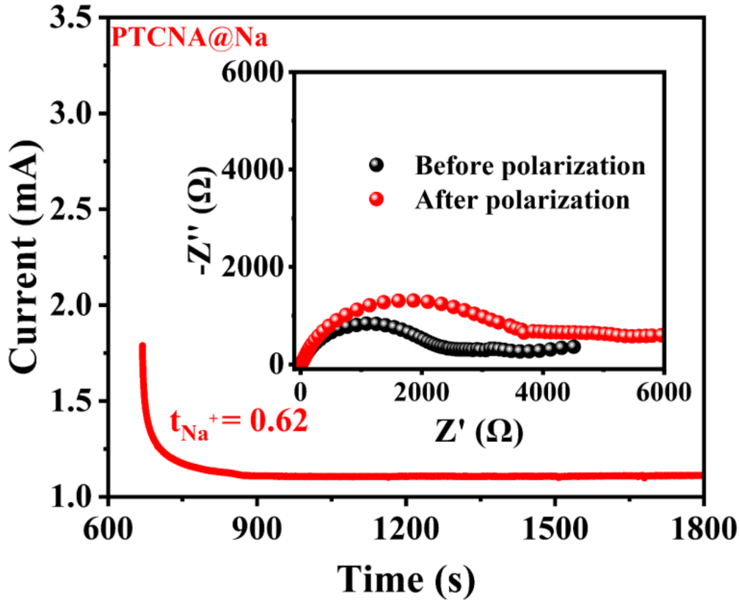

Fig. S44 The Na$^+$ transference number of PTCNA@Na.

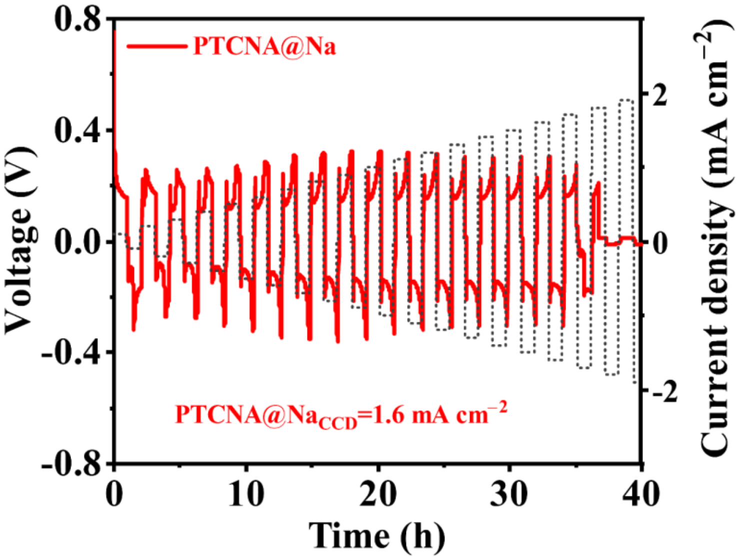

Fig. S45 The CCD text of PTCNA@Na.

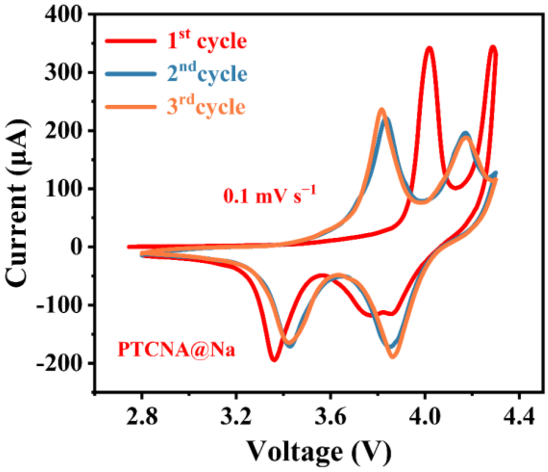

Fig. S46 The CV curves of Li|PTCNA@Na|NVPF cells cycled for three cycles at a sweep rate of 0.1 mV s^{-1}.

Table S1. The comprehensive performance of PVDF-based electrolytes achieved in this work is compared with that reported in previous studies.

Electrolytes	**Li||Li cells cycle life (h)**	**Full cells test temperature range (°C)**	**The type of cathode tested**	**Maximum cutoff voltage tested for full cell (V)**	**Maximum loading tested with full cells (mg cm^{-2})**	**Ref.**
This work	**7000 (0.1 mA cm^{-2} at –30 °C)**	**From –30 to 60**	**LFP, LCO, NCM811, and NCM9055**	**4.5 (LCO)**	**10.2 (NCM9055)**	/
PVDF−PZT CPE	1900 (0.1 mA cm^{-2} at 25 °C)	25	NCM811	4.3 (NCM811)	1 (NCM811)	S12
PVDF:LLZTO-P	1000 (0.1 mA cm^{-2} at 30 °C)	30	LFP, and NCM622	4.2 (NCM622)	3 (LFP/NCM622)	S13
PV-MS20	5100 (0.1 mA cm^{-2} at 28 °C)	28	NCM811	4.5 (NCM811)	1.8 (NCM811)	S14
PVDF-OCN	2500 (0.1 mA cm^{-2} at 25 °C)	25	NCM811	4.3 (NCM811)	8.2 (NCM811)	S15
PVBL	1900 (0.1 mA cm^{-2} at 25 °C)	From –20 to 25	NCM811	4.3 (NCM811)	5 (NCM811)	S16
PTC ionic-SPE	1500 (0.1 mA cm^{-2} at 25 °C)	25	LFP, and NCM811	4.3 (NCM811)	10.4 (LFP)	S17
PVMS-15	1900 (0.1 mA cm^{-2} at 25 °C)	From –20 to 45	NCM811	4.5 (NCM811)	8 (NCM811)	S18
PVHLL	2000 (0.25 mA cm^{-2} at 25 °C)	25	LFP	3.8 (LFP)	2 (LFP)	S19

PPM	3200 (0.1 mA cm^{-2} at 25 °C)	From –30 to 25	NCM811	4.3 (NCM811)	9 (NCM811)	S20
β-PVDF-HFP	4000 (0.1 mA cm^{-2} at 25 °C)	25	LFP, LCO, NCM622, and NCM92	4.3 (LCO/NCM622)	9.6 (LFP)	S21
PTDB SPE	5000 (0.2 mA cm^{-2} at 25 °C)	25	LFP, and NCM811	4.4 (NCM811)	3 (NCM811)	S22
PLLDB	1800 (0.05 mA cm^{-2} at 25 °C)	25	LFP, and NCM811	4.3 (NCM811)	2 (LFP/NCM811)	S23
PNNO-5	2800 (0.1 mA cm^{-2} at 25 °C)	From –20 to 25	NCM811	4.3 (NCM811)	10 (NCM811)	S24
Zr-F4	2000 (1 mA cm^{-2} at 25 °C)	25	LFP, and NCM811	4.5 (NCM811)	6.82 (LFP)	S25

Supplementary References

1. X. Wang, L. Yang, N. Ahmad, L. Ran, R. Shao and W. Yang, *Adv. Mater.*, 2023, **35**, 2209140.
2. B. Ravel and M. Newville, *J. Synchrotron Radiat.*, 2005, **12**, 537-541.
3. N. Sieffert and G. Wipff, *Dalton Trans.*, 2015, **44**, 2623-2638.
4. A. D. Becke, *J. Chem. Phys.*, 1992, **96**, 2155-2160.
5. P. Giannozzi, O. Andreussi, T. Brumme, O. Bunau, M. B. Nardelli, M. Calandra, R. Car, C. Cavazzoni, D. Ceresoli, M. Cococcioni, N. Colonna, I. Carnimeo, A. Dal Corso, S. de Gironcoli, P. Delugas, R. A. DiStasio, Jr., A. Ferretti, A. Floris, G. Fratesi, G. Fugallo, R. Gebauer, U. Gerstmann, F. Giustino, T. Gorni, J. Jia, M. Kawamura, H. Y. Ko, A. Kokalj, E. Kucukbenli, M. Lazzeri, M. Marsili, N. Marzari, F. Mauri, N. L. Nguyen, H. V. Nguyen, A. Otero-de-la-Roza, L. Paulatto, S. Ponce, D. Rocca, R. Sabatini, B. Santra, M. Schlipf, A. P. Seitsonen, A. Smogunov, I. Timrov, T. Thonhauser, P. Umari, N. Vast, X. Wu and S. Baroni, *J. Condens. Matter Phys.*, 2017, **29**, 465901.
6. P. Giannozzi, S. Baroni, N. Bonini, M. Calandra, R. Car, C. Cavazzoni, D. Ceresoli, G. L. Chiarotti, M. Cococcioni, I. Dabo, A. Dal Corso, S. de Gironcoli, S. Fabris, G. Fratesi, R. Gebauer, U. Gerstmann, C. Gougoussis, A. Kokalj, M. Lazzeri, L. Martin-Samos, N. Marzari, F. Mauri, R. Mazzarello, S. Paolini, A. Pasquarello, L. Paulatto, C. Sbraccia, S. Scandolo, G. Sclauzero, A. P. Seitsonen, A. Smogunov, P. Umari and R. M. Wentzcovitch, *J. Condens. Matter Phys.*, 2009, **21**, 395502.
7. J. Paier, R. Hirschl, M. Marsman and G. Kresse, *J. Chem. Phys.*, 2005, **122**, 234102.
8. Perdew, Burke and Ernzerhof, *Phys. Rev. Lett.*, 1996, **77**, 3865-3868.
9. M. Zhou, Y. Zhang, H. Li, Z. Li, S. Wang, X. Lu and S. Yang, *Angew. Chem. Int. Ed.*, 2025, **64**, e202414392.
10. H. Wang, H. Sui, Y. Ding, Y. Yang, Y. Su and H. Li, *J. Am. Chem. Soc.*, 2025, **147**, 6095-6107.
11. Z. Lu, D. Liu, K. Dai, K. Liu, C. Jing, W. He, W. Wang, C. Zhang and W. Wei, *Energy Storage Mater.*, 2023, **57**, 316-325.
12. B.-H. Kang, S.-F. Li, J. Yang, Z.-M. Li and Y.-F. Huang, *ACS Nano*, 2023, **17**, 14114-14122.
13. N. Wang, M. Jia, Z. Bi and X. Guo, *Adv. Funct. Mater.*, 2024, **34**, 2401400.
14. W. Yang, Y. Liu, X. Sun, Z. He, P. He and H. Zhou, *Angew. Chem. Int. Ed.*, 2024, **63**, e202401428.
15. M. Shen, Y. Wei, M. Ge, S. Yu, R. Dou, L. Chen, F. Wang, Y. Huang and H. Xu, *Interd. Mater.*, 2024, **3**, 791-800.
16. P. Shi, J. Ma, M. Liu, S. Guo, Y. Huang, S. Wang, L. Zhang, L. Chen, K. Yang, X. Liu, Y. Li, X. An, D. Zhang, X. Cheng, Q. Li, W. Lv, G. Zhong, Y.-B. He and F. Kang, *Nat. Nanotechnol.*, 2023, **18**, 602-610.
17. J. F. Liu, Z. Y. Wu, F. J. Stadler and Y. F. Huang, *Angew. Chem. Int. Ed.*, 2023, **62**, e202300243.
18. Q. Wu, M. Fang, S. Jiao, S. Li, S. Zhang, Z. Shen, S. Mao, J. Mao, J. Zhang, Y. Tan, K. Shen, J. Lv, W. Hu, Y. He and Y. Lu, *Nat. Commun.*, 2023, **14**, 6296.
19. J. Lu, B. Sheng, M. Chen, M. Xu, Y. Zhang, S. Zhao, Q. Zhou, C. Li, B. Wang, J. Liu, J. Chen, Z. Lou and X. Han, *Energy Storage Mater.*, 2024, **71**, 103570.
20. Y. Ma, Y. Qiu, K. Yang, S. Lv, Y. Li, X. An, G. Xiao, Z. Han, Y. Ma, L. Chen, D. Zhang, W. Lv, Y. Tian, T. Hou, M. Liu, Z. Zhou, F. Kang and Y.-B. He, *Energy Environ. Sci.*, 2024, **17**, 8274-8283.
21. S. Wang, C. Li, Y. Ma, H. Zhang, X. Shi, L. Zhang and D. Song, *Angew. Chem. Int. Ed.*, 2024, **64**, e20242069.
22. Y. Zhang, H. Liu, F. Liu, S. Zhang, M. Zhou, Y. Liao, Y. Wei, W. Dong, T. Li, C. Liu, Q. Liu, H. Xu, G. Sun, Z. Wang, Y. Ren and J. Yang, *ACS Nano*, 2025, **19**, 3197-3209.
23. M. Li, H. An, Y. Song, Q. Liu, J. Wang, H. Huo, S. Lou and J. Wang, *J. Am. Chem. Soc.*, 2023, **145**, 25632-25642.
24. X. An, Y. Liu, K. Yang, J. Mi, J. Ma, D. Zhang, L. Chen, X. Liu, S. Guo, Y. Li, Y. Ma, M. Liu, Y.-B. He and F. Kang, *Adv. Mater.*, 2024, **36**, 2311195.
25. W. Huang, S. Wang, X. Zhang, Y. Kang, H. Zhang, N. Deng, Y. Liang and H. Pang, *Adv. Mater.*, 2023, **35**, 2310147.